# Search for $XYZ$ states in $\Upsilon(1S)$ inclusive decays

C. P. Shen,[2] C. Z. Yuan,[20] Y. Ban,[51] H. Aihara,[65] D. M. Asner,[50] I. Badhrees,[59,27] A. M. Bakich,[58] E. Barberio,[37] P. Behera,[18] V. Bhardwaj,[15] B. Bhuyan,[17] J. Biswal,[24] A. Bondar,[3,49] G. Bonvicini,[69] A. Bozek,[47] M. Bračko,[35,24] T. E. Browder,[12] D. Červenkov,[4] V. Chekelian,[36] A. Chen,[44] B. G. Cheon,[11] K. Chilikin,[32,39] R. Chistov,[32,39] K. Cho,[28] V. Chobanova,[36] S.-K. Choi,[10] Y. Choi,[57] D. Cinabro,[69] J. Dalseno,[36,61] M. Danilov,[39,32] N. Dash,[16] S. Di Carlo,[69] Z. Doležal,[4] Z. Drásal,[4] D. Dutta,[60] S. Eidelman,[3,49] H. Farhat,[69] J. E. Fast,[50] T. Ferber,[7] B. G. Fulsom,[50] V. Gaur,[60] N. Gabyshev,[3,49] A. Garmash,[3,49] P. Goldenzweig,[26] J. Haba,[13,9] K. Hayasaka,[48] H. Hayashii,[43] W.-S. Hou,[46] T. Iijima,[42,41] G. Inguglia,[7] A. Ishikawa,[63] R. Itoh,[13,9] W. W. Jacobs,[19] H. B. Jeon,[30] K. K. Joo,[5] T. Julius,[37] K. H. Kang,[30] D. Y. Kim,[56] J. B. Kim,[29] K. T. Kim,[29] S. H. Kim,[11] Y. J. Kim,[28] K. Kinoshita,[6] P. Kodyš,[4] S. Korpar,[35,24] D. Kotchetkov,[12] P. Križan,[33,24] P. Krokovny,[3,49] T. Kuhr,[34] A. Kuzmin,[3,49] Y.-J. Kwon,[71] J. S. Lange,[8] C. H. Li,[37] H. Li,[19] L. Li,[53] Y. Li,[68] L. Li Gioi,[36] J. Libby,[18] D. Liventsev,[68,13] T. Luo,[52] M. Masuda,[64] T. Matsuda,[38] D. Matvienko,[3,49] A. Moll,[36,61] H. K. Moon,[29] R. Mussa,[23] M. Nakao,[13,9] T. Nanut,[24] K. J. Nath,[17] Z. Natkaniec,[47] M. Nayak,[69] K. Negishi,[63] S. Nishida,[13,9] S. Ogawa,[62] S. Okuno,[25] S. L. Olsen,[54] P. Pakhlov,[32,39] G. Pakhlova,[32,40] B. Pal,[6] R. Pestotnik,[24] M. Petrič,[24] L. E. Piilonen,[68] C. Pulvermacher,[26] M. Ritter,[34] A. Rostomyan,[7] Y. Sakai,[13,9] S. Sandilya,[6] L. Santelj,[13] T. Sanuki,[63] V. Savinov,[52] T. Schlüter,[34] O. Schneider,[31] G. Schnell,[1,14] C. Schwanda,[21] Y. Seino,[48] K. Senyo,[70] O. Seon,[41] I. S. Seong,[12] M. E. Sevior,[37] T.-A. Shibata,[66] J.-G. Shiu,[46] F. Simon,[36,61] A. Sokolov,[22] E. Solovieva,[32,40] M. Starič,[24] T. Sumiyoshi,[67] M. Takizawa,[55] K. Tanida,[54] F. Tenchini,[37] K. Trabelsi,[13,9] M. Uchida,[66] T. Uglov,[32,40] Y. Unno,[11] S. Uno,[13,9] G. Varner,[12] A. Vinokurova,[3,49] V. Vorobyev,[3,49] C. H. Wang,[45] M.-Z. Wang,[46] P. Wang,[20] X. L. Wang,[68] M. Watanabe,[48] Y. Watanabe,[25] K. M. Williams,[68] E. Won,[29] J. Yamaoka,[50] S. D. Yang,[51] S. Yashchenko,[7] Y. Yook,[71] Y. Yusa,[48] Z. P. Zhang,[53] V. Zhilich,[3,49] V. Zhukova,[39] V. Zhulanov,[3,49] and A. Zupanc[33,24]

(Belle Collaboration)

[1]*University of the Basque Country UPV/EHU, 48080 Bilbao*
[2]*Beihang University, Beijing 100191*
[3]*Budker Institute of Nuclear Physics SB RAS, Novosibirsk 630090*
[4]*Faculty of Mathematics and Physics, Charles University, 121 16 Prague*
[5]*Chonnam National University, Kwangju 660-701*
[6]*University of Cincinnati, Cincinnati, Ohio 45221*
[7]*Deutsches Elektronen–Synchrotron, 22607 Hamburg*
[8]*Justus-Liebig-Universität Gießen, 35392 Gießen*
[9]*SOKENDAI (The Graduate University for Advanced Studies), Hayama 240-0193*
[10]*Gyeongsang National University, Chinju 660-701*
[11]*Hanyang University, Seoul 133-791*
[12]*University of Hawaii, Honolulu, Hawaii 96822*
[13]*High Energy Accelerator Research Organization (KEK), Tsukuba 305-0801*
[14]*IKERBASQUE, Basque Foundation for Science, 48013 Bilbao*
[15]*Indian Institute of Science Education and Research Mohali, SAS Nagar, 140306*
[16]*Indian Institute of Technology Bhubaneswar, Satya Nagar 751007*
[17]*Indian Institute of Technology Guwahati, Assam 781039*
[18]*Indian Institute of Technology Madras, Chennai 600036*
[19]*Indiana University, Bloomington, Indiana 47408*
[20]*Institute of High Energy Physics, Chinese Academy of Sciences, Beijing 100049*
[21]*Institute of High Energy Physics, Vienna 1050*
[22]*Institute for High Energy Physics, Protvino 142281*
[23]*INFN—Sezione di Torino, 10125 Torino*
[24]*J. Stefan Institute, 1000 Ljubljana*
[25]*Kanagawa University, Yokohama 221-8686*
[26]*Institut für Experimentelle Kernphysik, Karlsruher Institut für Technologie, 76131 Karlsruhe*
[27]*King Abdulaziz City for Science and Technology, Riyadh 11442*
[28]*Korea Institute of Science and Technology Information, Daejeon 305-806*
[29]*Korea University, Seoul 136-713*
[30]*Kyungpook National University, Daegu 702-701*
[31]*École Polytechnique Fédérale de Lausanne (EPFL), Lausanne 1015*
[32]*P.N. Lebedev Physical Institute of the Russian Academy of Sciences, Moscow 119991*
[33]*Faculty of Mathematics and Physics, University of Ljubljana, 1000 Ljubljana*
[34]*Ludwig Maximilians University, 80539 Munich*
[35]*University of Maribor, 2000 Maribor*

 © 2016 American Physical Society

[36]*Max-Planck-Institut für Physik, 80805 München*
[37]*School of Physics, University of Melbourne, Victoria 3010*
[38]*University of Miyazaki, Miyazaki 889-2192*
[39]*Moscow Physical Engineering Institute, Moscow 115409*
[40]*Moscow Institute of Physics and Technology, Moscow Region 141700*
[41]*Graduate School of Science, Nagoya University, Nagoya 464-8602*
[42]*Kobayashi-Maskawa Institute, Nagoya University, Nagoya 464-8602*
[43]*Nara Women's University, Nara 630-8506*
[44]*National Central University, Chung-li 32054*
[45]*National United University, Miao Li 36003*
[46]*Department of Physics, National Taiwan University, Taipei 10617*
[47]*H. Niewodniczanski Institute of Nuclear Physics, Krakow 31-342*
[48]*Niigata University, Niigata 950-2181*
[49]*Novosibirsk State University, Novosibirsk 630090*
[50]*Pacific Northwest National Laboratory, Richland, Washington 99352*
[51]*Peking University, Beijing 100871*
[52]*University of Pittsburgh, Pittsburgh, Pennsylvania 15260*
[53]*University of Science and Technology of China, Hefei 230026*
[54]*Seoul National University, Seoul 151-742*
[55]*Showa Pharmaceutical University, Tokyo 194-8543*
[56]*Soongsil University, Seoul 156-743*
[57]*Sungkyunkwan University, Suwon 440-746*
[58]*School of Physics, University of Sydney, New South Wales 2006*
[59]*Department of Physics, Faculty of Science, University of Tabuk, Tabuk 71451*
[60]*Tata Institute of Fundamental Research, Mumbai 400005*
[61]*Excellence Cluster Universe, Technische Universität München, 85748 Garching*
[62]*Toho University, Funabashi 274-8510*
[63]*Department of Physics, Tohoku University, Sendai 980-8578*
[64]*Earthquake Research Institute, University of Tokyo, Tokyo 113-0032*
[65]*Department of Physics, University of Tokyo, Tokyo 113-0033*
[66]*Tokyo Institute of Technology, Tokyo 152-8550*
[67]*Tokyo Metropolitan University, Tokyo 192-0397*
[68]*Virginia Polytechnic Institute and State University, Blacksburg, Virginia 24061*
[69]*Wayne State University, Detroit, Michigan 48202*
[70]*Yamagata University, Yamagata 990-8560*
[71]*Yonsei University, Seoul 120-749*

(Received 3 May 2016; published 22 June 2016)

The branching fractions of the $\Upsilon(1S)$ inclusive decays into final states with a $J/\psi$ or a $\psi(2S)$ are measured with improved precision to be $\mathcal{B}(\Upsilon(1S) \to J/\psi + \text{anything}) = (5.25 \pm 0.13(\text{stat}) \pm 0.25(\text{syst})) \times 10^{-4}$ and $\mathcal{B}(\Upsilon(1S) \to \psi(2S) + \text{anything}) = (1.23 \pm 0.17(\text{stat}) \pm 0.11(\text{syst})) \times 10^{-4}$. The first search for $\Upsilon(1S)$ decays into $XYZ$ states that decay into a $J/\psi$ or a $\psi(2S)$ plus one or two charged tracks yields no significant signals for $XYZ$ states in any of the examined decay modes, and upper limits on their production rates in $\Upsilon(1S)$ inclusive decays are determined.

DOI: 10.1103/PhysRevD.93.112013

During the past 12 years, many charmoniumlike states, the so-called "$XYZ$" particles, have been reported [1]. Most cannot be described well by quarkonium potential models [1–3]. Their unusual properties have stimulated considerable theoretical interest and various interpretations have been proposed, including tetraquarks, molecules, hybrids, or hadrocharmonia [1,3,4]. To distinguish among these explanations, more experimental information is needed, such as additional production processes and/or more decay modes for these states. States with $J^{PC} = 1^{--}$ can be studied with initial state radiation in Belle's and *BABAR*'s large $\Upsilon(4S)$ data samples or via direct production in $e^+e^-$ collisions at BESIII. There is very little available information on $XYZ$ production in the decays of narrow $\Upsilon$ states apart from the searches for charge-parity-even charmoniumlike states in $\Upsilon(1S)$ [5] and $\Upsilon(2S)$ [6] radiative decays. A common feature of these $XYZ$ states is that they decay into a charmonium state such as $J/\psi$ or $\psi(2S)$ and light hadrons. Inclusive decays of $\Upsilon(1S)$ into $J/\psi$ and $\psi(2S)$ are observed with large branching fractions of $(6.5 \pm 0.7) \times 10^{-4}$ [7,8] and $(2.7 \pm 0.9) \times 10^{-4}$ [7], respectively, in which some of the

$XYZ$ states might have been produced before decaying into $J/\psi$ or $\psi(2S)$.

In this paper, we report a search for some of the $XYZ$ states in $\Upsilon(1S)$ inclusive decays using the world's largest data sample of $\Upsilon(1S)$. In these searches, 14 decay modes are considered: $X(3872)$ [9] and $Y(4260)$ [10] to $\pi^+\pi^- J/\psi$; $Y(4260)$ [11], $Y(4360)$ [12] and $Y(4660)$ [13] to $\pi^+\pi^-\psi(2S)$; $Y(4260)$ [14] to $K^+K^- J/\psi$; $Y(4140)$ [15] and $X(4350)$ [16] to $\phi J/\psi$; $Z_c(3900)^\pm$ [17,18], $Z_c(4200)^\pm$ [19] and $Z_c(4430)^\pm$ [19] to $\pi^\pm J/\psi$; $Z_c(4050)^\pm$ [11] and $Z_c(4430)^\pm$ [20] to $\pi^\pm\psi(2S)$; and a predicted $Z_{cs}^\pm$ state with mass $(3.97 \pm 0.08)$ GeV/$c^2$ and width $(24.9 \pm 12.6)$ MeV [21,22] to $K^\pm J/\psi$.

The analysis utilizes a 5.74 fb$^{-1}$ data sample collected at the peak of the $\Upsilon(1S)$ resonance, containing $102 \times 10^6$ $\Upsilon(1S)$ decays, and a 89.45 fb$^{-1}$ data sample collected off-resonance at $\sqrt{s} = 10.52$ GeV that is used to determine the levels of possible irreducible continuum contributions. The data were collected with the Belle detector [23,24] operated at the KEKB asymmetric-energy $e^+e^-$ collider [25,26]. Large Monte Carlo (MC) event samples of each of the investigated $XYZ$ modes are generated with EVTGEN [27] to determine signal line shapes and efficiencies. Both $XYZ$ meson production in $\Upsilon(1S)$ inclusive decays and their decays into exclusive final states containing a $J/\psi(\psi(2S))$ and light hadrons are generated uniformly in phase space. Inclusive $J/\psi(\psi(2S))$ production is generated in the same models and subsequently decay according to their known branching fractions [28]; unknown decay modes are generated using the Lund fragmentation model in PYTHIA [29].

The Belle detector is a large solid angle magnetic spectrometer that consists of a silicon vertex detector, a 50-layer central drift chamber (CDC), an array of aerogel threshold Cherenkov counters (ACC), a barrel-like arrangement of time-of-flight scintillation counters (TOF), and an electromagnetic calorimeter comprised of CsI(Tl) crystals (ECL) located inside a superconducting solenoid coil that provides a 1.5 T magnetic field. An iron flux-return yoke located outside the coil is instrumented to detect $K_L^0$ mesons and to identify muons. A detailed description of the Belle detector can be found in Refs. [23,24].

Charged tracks from the primary vertex with $dr < 2$ cm and $|dz| < 4$ cm are selected, where $dr$ and $dz$ are the impact parameters perpendicular to and along the beam direction, respectively, with respect to the interaction point. In addition, the transverse momentum of every charged track in the laboratory frame is restricted to be larger than 0.1 GeV/$c$. Backgrounds from QED processes are significantly suppressed by the requirement that the charged multiplicity ($N_{\rm ch}$) in each event satisfies $N_{\rm ch} > 4$ [30]. For charged tracks, information from different detector subsystems including specific ionization in the CDC, time measurements in the TOF and the response of the ACC is combined to form the likelihood $\mathcal{L}_i$ for particle species $i$, where $i = \pi$, $K$ or $p$ [31]. Charged tracks with $R_K = \mathcal{L}_K/(\mathcal{L}_K + \mathcal{L}_\pi) > 0.6$ are treated as kaons, while those with $R_K < 0.4$ are considered to be pions. With these conditions, the kaon (pion) identification efficiency is 94% (97%) and the pion (kaon) misidentification rate is about 4% (9%). Candidate lepton tracks from $J/\psi(\psi(2S))$ are required to have a muon likelihood ratio $R_\mu = \mathcal{L}_\mu/(\mathcal{L}_\mu + \mathcal{L}_K + \mathcal{L}_\pi) > 0.1$ [32] or an electron likelihood ratio $R_e = \mathcal{L}_e/(\mathcal{L}_e + \mathcal{L}_{\rm non-}e) > 0.01$ [33]. Furthermore, we require that a charged pion not be identified as a muon or an electron with $R_\mu < 0.95$ and $R_e < 0.95$.

To reduce the effect of bremsstrahlung and final-state radiation, photons detected in the ECL within a 50 mrad cone of the original electron or positron direction are included in the calculation of the $e^+/e^-$ four-momentum. The lepton-identification efficiencies for $e^\pm$ and $\mu^\pm$ are about 98% and 96%, respectively.

Since a final-state $J/\psi$ or $\psi(2S)$ is common to all of the studies reported here, we first select either a $J/\psi$ via its $\ell^+\ell^-$ ($\ell = e$ or $\mu$) decay mode or a $\psi(2S)$ decaying into $\ell^+\ell^-$ or $\pi^+\pi^- J/\psi$. For $\psi(2S) \to \pi^+\pi^- J/\psi$, a mass-constrained fit is applied to the $J/\psi$ candidate.

After all the event selection requirements, significant $J/\psi(\to \ell^+\ell^-)$, $\psi(2S)(\to \ell^+\ell^-)$, and $\psi(2S)(\to \pi^+\pi^- J/\psi)$ signals are seen in the $\Upsilon(1S)$ data sample, as shown in Fig. 1. The shaded histograms in this figure are the normalized continuum backgrounds that are determined from the $\sqrt{s} = 10.52$ GeV continuum data sample and extrapolated down to the $\Upsilon(1S)$ resonance energy. The scale factor used for this extrapolation is $f_{\rm scale} = \mathcal{L}_\Upsilon/\mathcal{L}_{\rm con} \times \sigma_\Upsilon/\sigma_{\rm con} \times \varepsilon_\Upsilon/\varepsilon_{\rm con}$, where $\mathcal{L}_\Upsilon/\mathcal{L}_{\rm con}$, $\sigma_\Upsilon/\sigma_{\rm con}$, and $\varepsilon_\Upsilon/\varepsilon_{\rm con}$ are the ratios of the integrated luminosities, cross sections, and efficiencies, respectively, for the $\Upsilon(1S)$ and continuum samples. The MC-determined efficiencies for the $\Upsilon(1S)$ and continuum data samples are found to be nearly the same for all the decay modes, and the dependence of the cross sections on $s$ is assumed to be proportional to $1/s^2$ [34–36]. The resulting scale factor is 0.098.

Considering the slight differences in the MC-determined reconstruction efficiencies for different $J/\psi(\psi(2S))$ momenta, we partition the data samples according to the scaled momentum $x = p_\psi^*/(\frac{1}{2\sqrt{s}} \times (s - m_\psi^2))$ [7], where the subscript $\psi$ represents $J/\psi$ ($\psi(2S)$), $p_\psi^*$ is the momentum of the $\psi$ candidate in the $e^+e^-$ center-of-mass system, and $m_\psi$ is the $\psi$ mass [28]. The value of $(\frac{1}{2\sqrt{s}} \times (s - m_\psi^2))$ is the value of $p_\psi^*$ for the case where the $\psi$ candidate recoils against a massless particle. The use of $x$ removes the beam-energy dependence in comparing the continuum data to that taken at the $\Upsilon(1S)$ resonance.

An unbinned extended simultaneous likelihood fit is applied to the $x$-dependent $J/\psi(\psi(2S))$ spectra to extract the signal yields in the $\Upsilon(1S)$ and continuum data samples. Due to the slight dependence on momentum, the $J/\psi(\psi(2S))$ signal shape is directly obtained from the MC

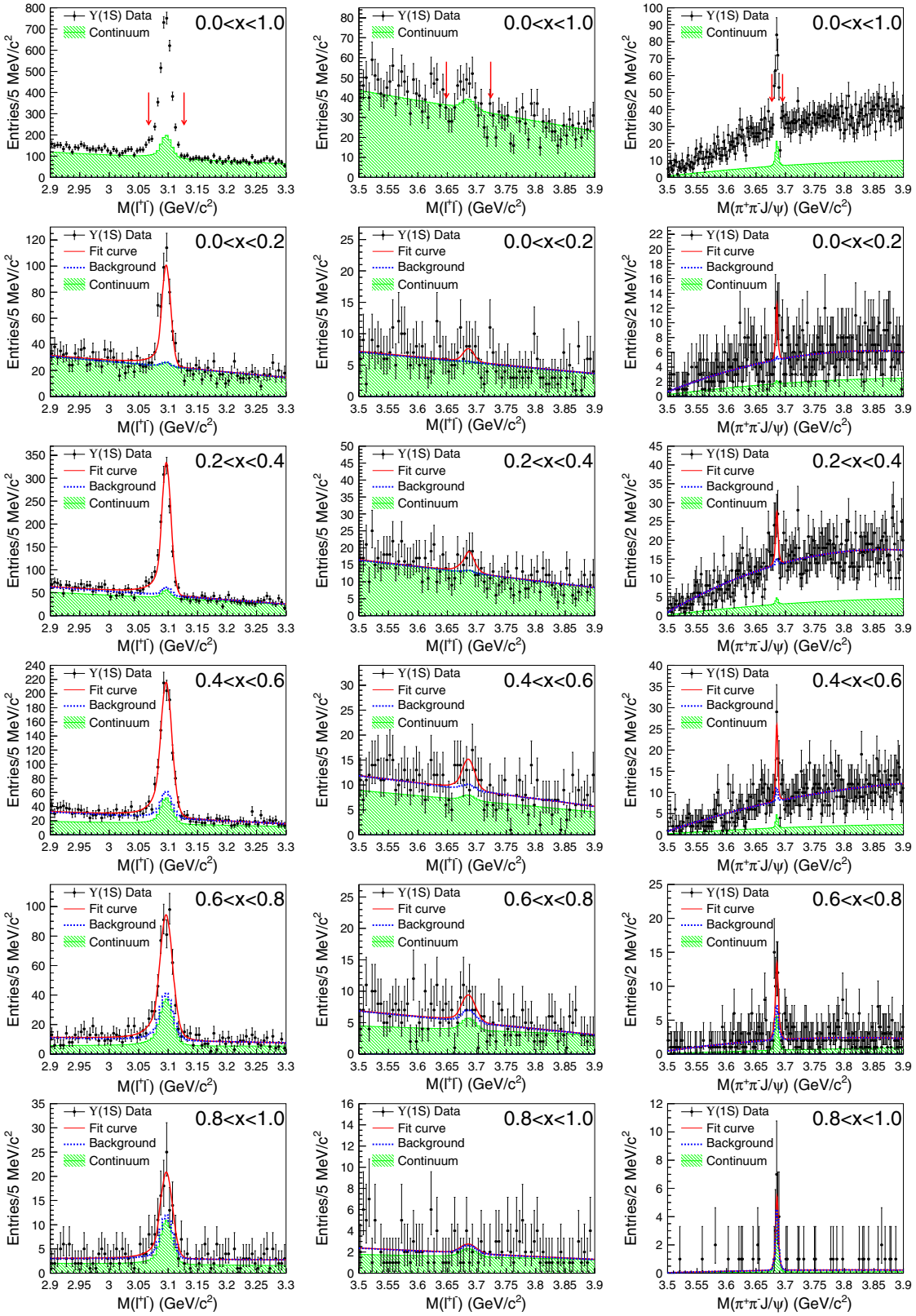



FIG. 1. Invariant mass distributions of the $J/\psi(\to \ell^+\ell^-)$ (left column), $\psi(2S)(\to \ell^+\ell^-)$ (middle column), and $\psi(2S)(\to \pi^+\pi^- J/\psi)$ (right column) candidates in the entire $x$ region (top row) and for $x$ bins of size 0.2 (remaining rows). The points with error bars are for the $\Upsilon(1S)$ data sample; the shaded histograms are the continuum contributions scaled from the $\sqrt{s} = 10.52$ GeV data sample. The solid lines are the best fit with the total fitted background components represented by the dashed lines. The $J/\psi$ and $\psi(2S)$ signal regions used for the $XYZ$ searches are indicated by the arrows in the top-row plots.

TABLE I. Summary of the branching fraction measurements of $\Upsilon(1S)$ inclusive decays into the $J/\psi(\psi(2S))$, where $N_{\rm fit}$ is the number of fitted signal events, $\varepsilon(\%)$ is the reconstruction efficiency with all intermediate-state branching fractions included, $\sigma_{\rm syst}(\%)$ is the total systematic error on the branching fraction measurement, and $\mathcal{B}$ is the measured branching fraction. For the $\psi(2S)$ channel, $\varepsilon$ is the sum of the reconstruction efficiencies in the $\ell^+\ell^-$ and $\pi^+\pi^- J/\psi$ decay modes with the branching fractions of the intermediate states included.

| | $\Upsilon(1S) \to J/\psi +$ anything | | | | $\Upsilon(1S) \to \psi(2S) +$ anything | | | |
|---|---|---|---|---|---|---|---|---|
| $x$ | $N_{\rm fit}$ | $\varepsilon(\%)$ | $\sigma_{\rm syst}(\%)$ | $\mathcal{B}(10^{-4})$ | $N_{\rm fit}$ | $\varepsilon(\%)$ | $\sigma_{\rm syst}(\%)$ | $\mathcal{B}(10^{-4})$ |
| (0.0,0.2) | $379.3 \pm 28.1$ | 6.06 | 4.3 | $0.61 \pm 0.05 \pm 0.03$ | $30.1 \pm 10.5$ | 1.81 | 21.8 | $0.16 \pm 0.06 \pm 0.04$ |
| (0.2,0.4) | $1297.6 \pm 48.6$ | 5.78 | 5.4 | $2.20 \pm 0.08 \pm 0.12$ | $71.3 \pm 18.3$ | 1.76 | 26.5 | $0.40 \pm 0.10 \pm 0.11$ |
| (0.4,0.6) | $904.6 \pm 41.6$ | 5.51 | 5.6 | $1.61 \pm 0.07 \pm 0.09$ | $71.5 \pm 15.4$ | 1.68 | 18.6 | $0.42 \pm 0.09 \pm 0.08$ |
| (0.6,0.8) | $354.0 \pm 29.3$ | 5.15 | 6.8 | $0.67 \pm 0.06 \pm 0.05$ | $39.5 \pm 12.0$ | 1.65 | 16.6 | $0.23 \pm 0.07 \pm 0.04$ |
| (0.8,1.0) | $54.2 \pm 13.4$ | 3.36 | 7.6 | $0.16 \pm 0.04 \pm 0.02$ | $2.5 \pm 5.7$ | 1.40 | 78.4 | $0.02 \pm 0.04 \pm 0.02$ |
| Sum | $2989.6 \pm 75.0$ | 5.62 | 4.7 | $5.25 \pm 0.13 \pm 0.25$ | $214.9 \pm 29.3$ | 1.71 | 8.9 | $1.23 \pm 0.17 \pm 0.11$ |

simulation in each $x$ bin convolved with a Gaussian function with a free width in the fit to account for possible discrepancy between data and MC simulation. In the fit to the $\Upsilon(1S)$ candidates, a Chebyshev polynomial background shape is used for the $\Upsilon(1S)$ decay backgrounds in addition to the normalized continuum contribution. Particularly for the $\Upsilon(1S)$ to $\psi(2S)$ inclusive decays, the $\psi(2S) \to \ell^+\ell^-$ and $\psi(2S) \to \pi^+\pi^- J/\psi$ decay modes are treated together to obtain the total $\psi(2S)$ signal yield; that is to say, we apply an additional simultaneous fit to the $\psi(2S)$ candidates in the two decay modes with the fixed ratios of MC-determined efficiencies between them with all of the branching fractions of the intermediate states included.

The invariant mass distributions for the $J/\psi$ and $\psi(2S)$ candidates for the entire $x$ region and $\Delta x = 0.2$ bins are shown in Fig. 1 with the results of the fits to the spectra of the $J/\psi$ and $\psi(2S)$ candidates in $\Upsilon(1S)$ inclusive decays. The fitted signal yields ($N_{\rm fit}$) in each $x$ bin are tabulated in Table I, together with the reconstruction efficiencies ($\varepsilon$) [including all intermediate-state branching fractions], the total systematic uncertainties ($\sigma_{\rm syst}$), and the corresponding branching fractions ($\mathcal{B}$). The total systematic uncertainties

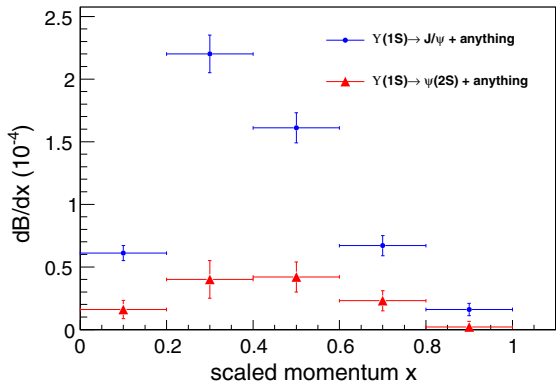



FIG. 2. Differential branching fractions for $\Upsilon(1S)$ inclusive decays into the $J/\psi$ and $\psi(2S)$ versus the scaled momentum $x$ defined in the text. For each point, the error is the sum of the statistical and systematic errors.

are the sum of the common systematic errors (described below) and fit errors estimated in each $x$ bin or the full range in $x$. The total numbers of $J/\psi(\psi(2S))$ events, *i.e.*, the sums of the signal yields in all of the $x$ bins, the sums of the $x$-dependent efficiencies weighted by the signal fraction in that $x$ bin, and the measured branching fraction values are also itemized in Table I. Our measurements are consistent with the PDG averages of previous results from CLEO-c, but with smaller central values and better precision. In addition, Fig. 2 shows the differential branching fractions of $\Upsilon(1S)$ inclusive decays into the $J/\psi$ and $\psi(2S)$.

We search for signals for certain $XYZ$ states by combining the $J/\psi(\psi(2S))$ with one or two light charged hadrons ($K^\pm/\pi^\pm$). MC simulations indicate that the mass resolutions of the $J/\psi(\psi(2S))$ candidates have a weak dependence on the production mode, so common signal and sideband regions are defined. In the $\phi J/\psi$ mode, the $\phi$ candidates are reconstructed in the $K^+K^-$ final state. For $J/\psi$, $\psi(2S)$ and $\phi$ candidates in their decay channels, the selected signal regions and the corresponding sidebands are summarized in Table II. All sidebands are defined to be twice as wide as the corresponding signal region. No peaking backgrounds or evident structures are found in these sideband events in any of the invariant mass distributions discussed below. To improve the mass resolutions of $XYZ$ candidates, vertex and mass-constrained fits are applied to the $J/\psi(\psi(2S))$ candidates; an

TABLE II. The definitions of the signal regions and the corresponding sidebands for (a) $J/\psi \to \ell^+\ell^-$, (b) $\psi(2S) \to \ell^+\ell^-$, (c) $\psi(2S) \to \pi^+\pi^- J/\psi$, and (d) $\phi \to K^+K^-$. The sidebands are selected to be twice as wide as the corresponding signal region.

| Channel | Signal region | Sidebands (GeV/$c^2$) |
|---|---|---|
| (a) | [3.067, 3.127] | [2.970, 3.030] or [3.170, 3.230] |
| (b) | [3.6485, 3.7235] | [3.535, 3.610] or [3.760, 3.835] |
| (c) | [3.677, 3.695] | [3.652, 3.670] or [3.700, 3.718] |
| (d) | [1.012, 1.027] | [0.989, 1.004] or [1.036, 1.051] |

unconstrained-mass vertex fit is done for the $\phi$ candidates since their natural width is larger than the mass resolution.

An unbinned extended simultaneous maximum likelihood fit to the mass distributions of the $XYZ$ candidates is performed to extract the signal and background yields in the $\Upsilon(1S)$ and continuum data samples. The signal shapes of the examined $XYZ$ states used in the fits are obtained directly from MC simulations that use world average values for their masses and widths [28]. In the fit to the $\Upsilon(1S)$ data sample, a Chebyshev polynomial function is used for the $\Upsilon(1S)$ decay backgrounds in addition to the normalized continuum contribution.

Figure 3 shows the $\pi^+\pi^- J/\psi$ invariant mass distributions, relevant for the $X(3872)$ and $Y(4260)$ searches, and those for $\pi^+\pi^-\psi(2S)$, relevant for the $Y(4260)$, $Y(4360)$ and $Y(4660)$. There are no evident signals for any of these states; the solid lines indicate the best fit results from a simultaneous fit to the $\Upsilon(1S)$ and continuum data samples. The dashed curves are the total background estimates. The same representations of the curves and histograms are used for the $K^+K^- J/\psi$ and $\phi J/\psi$ mass distributions shown in Figs. 4(a) and 5(a), respectively, and for the charged $\pi^\pm J/\psi(\psi(2S))$ and $K^\pm J/\psi$ modes in Figs. 6 and 7(a), respectively.

Because of the large difference between the $X(3872)$ and $Y(4260)$ widths [28], the fit range for the $M(\pi^+\pi^- J/\psi)$ spectrum is separated into low and high mass regions with different bin widths as shown in Figs. 3(a) and 3(b). The sharp peak at the $\psi(2S)$ nominal mass, as seen in Fig. 3(a), is from $\Upsilon(1S) \to \psi(2S) + \text{anything} \to \pi^+\pi^- J/\psi +$ anything. In contrast, no $X(3872)$ signal is observed. Using the MC-determined $\psi(2S)$ signal shape, the fit yields $139.8 \pm 20.2$ $\psi(2S)$ signal events. With the MC-determined reconstruction efficiency (0.98%), the resulting branching fraction of the $\Upsilon(1S)$ inclusive decay into $\psi(2S)$ is $(1.39 \pm 0.20(\text{stat}) \pm 0.13(\text{syst})) \times 10^{-4}$. The measurement is in agreement with that listed in Table I, where the $\psi(2S)$ candidates are reconstructed via $\ell^+\ell^-$ and $\pi^+\pi^- J/\psi$. In addition, there is no evidence for $Y(4260)$ signal in the $\pi^+\pi^- J/\psi$ mass spectrum shown in Fig. 3(b). We also search for the $Y(4260)$ state in the $\pi^+\pi^-\psi(2S)$ mass spectra shown in Figs. 3(c) and 3(d) for the $\ell^+\ell^-$ and $\pi^+\pi^- J/\psi$ decay modes, respectively, of the $\psi(2S)$ candidates, as well as the $Y(4360)$ and $Y(4660)$ states. No enhancements near the nominal masses of these states are evident.

The $Y(4260)$ has been seen in the $K^+K^- J/\psi$ channel by CLEO-c [14]. Figure 4(a) shows the $K^+K^- J/\psi$ invariant mass distributions for the candidate $\Upsilon(1S)$ inclusive decays. The fit to the spectrum of $M(K^+K^- J/\psi)$ is performed above 4.10 GeV/$c^2$, which is somewhat above the $K^+K^- J/\psi$ mass threshold of 4.085 GeV/$c^2$. The invariant mass distributions of the $K^+K^-\psi(2S)$ candidates in $\Upsilon(1S)$ inclusive decays are shown in Figs. 4(b) and 4(c) for $\psi(2S) \to \ell^+\ell^-$ and $\pi^+\pi^- J/\psi$, respectively. The slant-shaded histograms (the scaled continuum backgrounds) overlie the cross-shaded ones that represent the normalized $\psi(2S)$ mass sideband. No evidence is found for new structures or any of the known $XYZ$ states. The $Y(4140)$ and $X(4350)$ states have been reported in the $\phi J/\psi$ decay

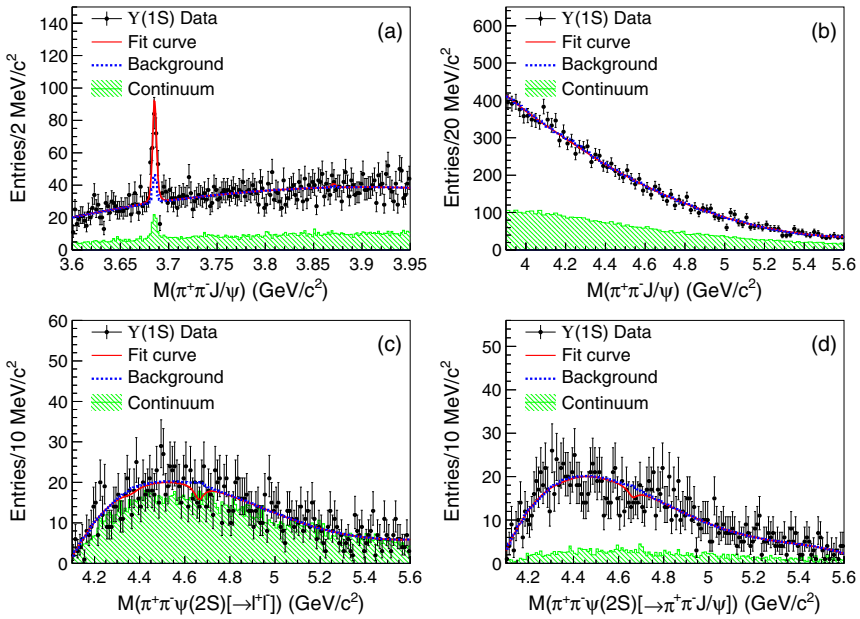



FIG. 3. The $\pi^+\pi^- J/\psi$ invariant mass distributions for the (a) lower- and (b) higher-mass regions; the (c) $\pi^+\pi^-\psi(2S)(\to \ell^+\ell^-)$ and (d) $\pi^+\pi^-\psi(2S)(\to \pi^+\pi^- J/\psi)$ invariant mass distributions. The points with error bars are the $\Upsilon(1S)$ events and the shaded histograms are the scaled continuum contributions determined from the data sample collected at $\sqrt{s} = 10.52$ GeV. The solid lines are the best fits with the total background components represented by the dashed lines.

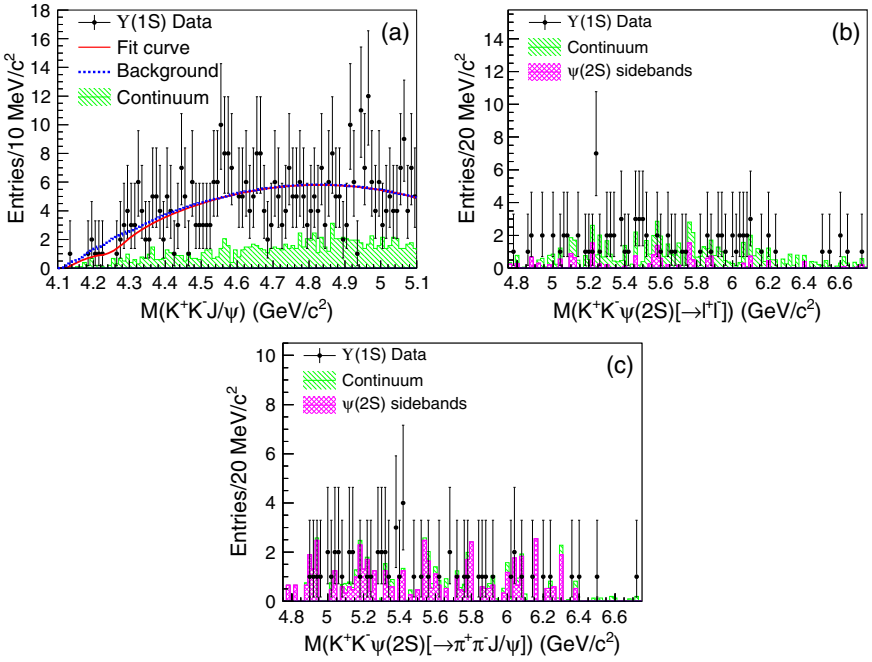



FIG. 4. Invariant mass distributions of the (a) $K^+K^-J/\psi$, (b) $K^+K^-\psi(2S)(\to \ell^+\ell^-)$, and (c) $K^+K^-\psi(2S)(\to \pi^+\pi^-J/\psi)$ candidates in $\Upsilon(1S)$ inclusive decays. The points with error bars are the $\Upsilon(1S)$ events and the slant-shaded histograms are the scaled continuum contributions with the data sample collected at $\sqrt{s} = 10.52$ GeV which overlie the normalized $\psi(2S)$ mass sideband backgrounds (the cross-shaded histograms) for the two $\psi(2S)$ decay modes. The solid line in panel (a) is the best fit with the fitted total background component represented as a dashed line.

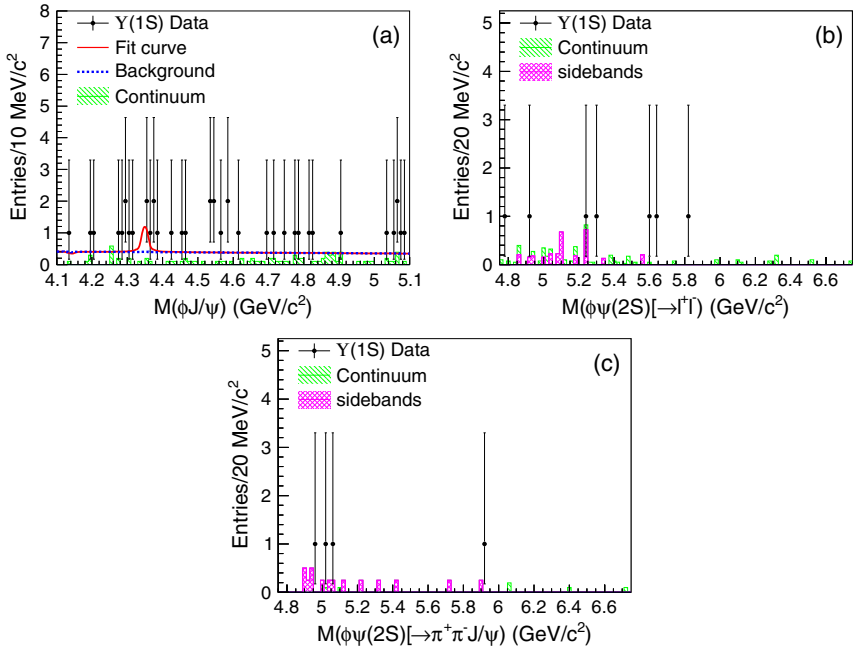



FIG. 5. Invariant mass distributions of the (a) $\phi J/\psi$, (b) $\phi\psi(2S)(\to \ell^+\ell^-)$, and (c) $\phi\psi(2S)(\to \pi^+\pi^-J/\psi)$ candidates in $\Upsilon(1S)$ inclusive decays. The points with error bars are events observed at the $\Upsilon(1S)$ peak, and the slant-shaded histograms are the scaled continuum contributions from the $\sqrt{s} = 10.52$ GeV continuum data sample which overlie the normalized $\psi(2S)$ mass sideband backgrounds (the cross-shaded histograms) for the two $\psi(2S)$ decay modes. The solid line in panel (a) is the best fit for the $\phi J/\psi$ mass spectrum and the dashed line is the total fitted background.

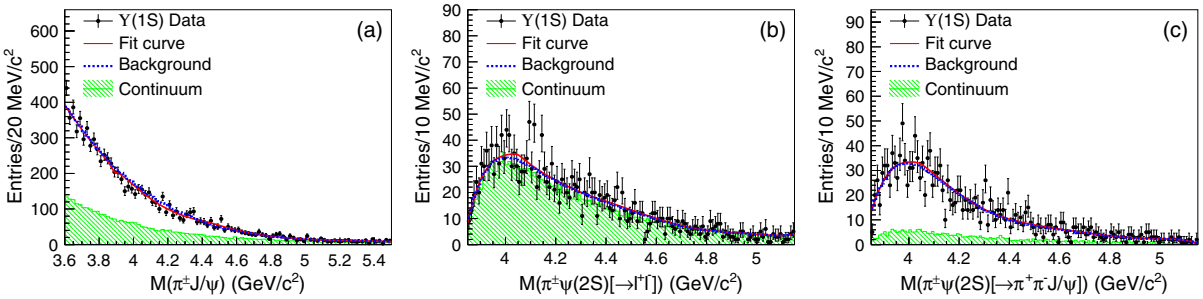



FIG. 6. Invariant mass distributions of the (a) $\pi^{\pm}J/\psi$, (b) $\pi^{\pm}\psi(2S)(\to \ell^+\ell^-)$, and (c) $\pi^{\pm}\psi(2S)(\to \pi^+\pi^- J/\psi)$ candidates in $\Upsilon(1S)$ inclusive decays. The points with error bars are the $\Upsilon(1S)$ events and the shaded histograms are the scaled continuum contributions with the data sample collected at $\sqrt{s} = 10.52$ GeV. The solid lines are the best fits with the fitted total background components represented by the dashed lines.

channel by CDF [15] and Belle [16]. Figure 5 shows the $\phi J/\psi$ and $\phi\psi(2S)$ invariant mass distributions, where the few events that survive do not appear to have any statistically significant clustering near 4140 MeV/$c^2$, 4350 MeV/$c^2$ nor any other mass. The results of a fit to $M(\phi J/\psi)$ in Fig. 5(a) are shown as a solid curve. Figures 5(b) and 5(c) show the $\phi\psi(2S)$ invariant mass distributions; there are only 7 and 4 events that survive in the $\ell^+\ell^-$ and $\pi^+\pi^- J/\psi$ decay modes, respectively. No structures are identified.

We search for various charged $Z_c^{\pm}$ states decaying into $\pi^{\pm}J/\psi(\psi(2S))$. Figure 6 shows the $\pi^{\pm}J/\psi$, $\pi^{\pm}\psi(2S)$ $(\to \ell^+\ell^-)$, and $\pi^{\pm}\psi(2S)(\to \pi^+\pi^- J/\psi)$ invariant mass distributions for the $\Upsilon(1S)$ peak data as well as the fit ranges and results. For all three channels, the background events represent the $\Upsilon(1S)$ data well, indicating insignificant production of any $Z_c^{\pm}$ states. We do not observe any $Z_c^{\pm}(3900)$, $Z_c^{\pm}(4200)$ or $Z_c^{\pm}(4430)$ signals in the $\pi^{\pm}J/\psi$ mode nor any $Z_c^{\pm}(4050)$ or $Z_c^{\pm}(4430)$ signals in the $\pi^{\pm}\psi(2S)$ mode. We search for the predicted $Z_{cs}^{\pm}(\to K^{\pm}J/\psi)$ state—the strange partner of $Z_c^{\pm}(3900)$ [21,22]—with mass $M = (3.97 \pm 0.08)$ GeV/$c^2$ and width $\Gamma = (24.9 \pm 12.6)$ MeV in $\Upsilon(1S)$ inclusive decays. The invariant mass distribution of the $K^{\pm}J/\psi$ candidates is presented in Fig. 7(a). No evidence for such a structure is seen near the predicted $Z_{cs}^{\pm}$ mass. The signal significance from the fit is less than $2\sigma$. A fit with a Breit-Wigner that interferes with a smooth background function yields a signal significance of only $1.2\sigma$. In the $K^{\pm}\psi(2S)$ mode, no exotic $XYZ$ states have been seen nor predicted. For completeness, we present the invariant mass distributions of the $K^{\pm}\psi(2S)$ candidates with the $\psi(2S)$ decays into the $\ell^+\ell^-$ and $\pi^+\pi^- J/\psi$ final states in Figs. 7(b) and 7(c), respectively. The sum of the normalized continuum and sideband backgrounds agrees well with the data.

The fitted signal yields ($N_{\rm fit}$) of the $XYZ$ states that are considered in this analysis are presented in Table III. Since the statistical significance in each case is less than $3\sigma$, upper limits on the number of signal events, $N_{\rm up}$, are determined at the 90% credibility level (C.L.) by solving the equation $\int_0^{N_{\rm up}} \mathcal{L}(x)dx / \int_0^{+\infty} \mathcal{L}(x)dx = 0.9$ [37], where $x$ is the number of fitted signal events and $\mathcal{L}(x)$ is the likelihood function in the fit to data. To take into account systematic uncertainties (discussed below), the above likelihood is convolved with a Gaussian function whose width equals the total systematic uncertainty. The calculated upper limits on the number of signal events ($N_{\rm up}$) and the branching

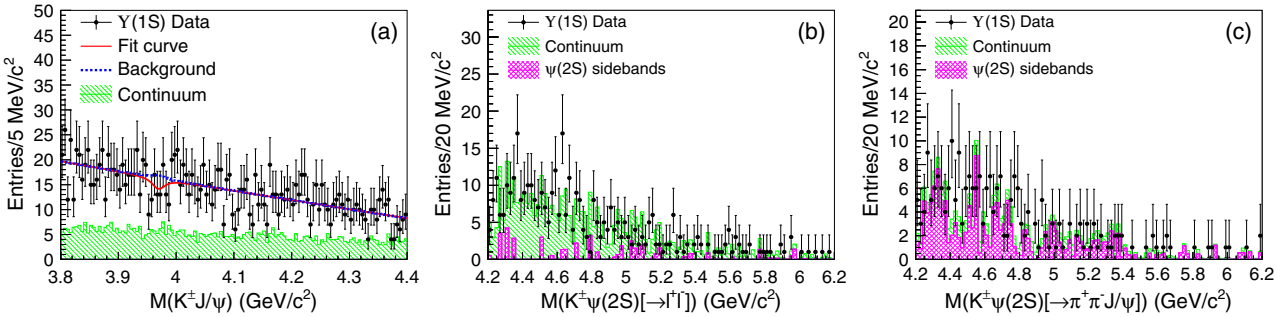



FIG. 7. The (a) $K^{\pm}J/\psi$, (b) $K^{\pm}\psi(2S)(\to \ell^+\ell^-)$, and (c) $K^{\pm}\psi(2S)(\to \pi^+\pi^- J/\psi)$ mass distributions for candidate events in the $\Upsilon(1S)$ peak decay sample. The points with error bars are the $\Upsilon(1S)$ events and the slant-shaded histograms are the scaled continuum contributions determined from the data collected at $\sqrt{s} = 10.52$ GeV. The normalized $\psi(2S)$ mass-sideband events are shown as the cross-shaded histograms. The solid line in panel (a) is the best fit with the fitted total background component represented by the dashed line.

TABLE III. Summary of the upper limits on the $\Upsilon(1S)$ inclusive decays into the exotic charmoniumlike states $XYZ$, where $N_{\rm fit}$ is the number of fitted signal events, $N_{\rm up}$ is the upper limit on the number of signal events taking into account systematic errors, $\varepsilon$ is the reconstruction efficiency, $\sigma_{\rm syst}$ is the total systematic uncertainty, $\Sigma$ is the signal significance with systematic errors included, and $\mathcal{B}_R^{\rm prod} = \mathcal{B}(\Upsilon(1S) \to XYZ + \text{anything})\mathcal{B}(XYZ \to J/\psi(\psi(2S)) + \text{hadrons})$ is the measured product branching fraction at the 90% C.L.

| State | $N_{\rm fit}$ | $N_{\rm up}$ | $\varepsilon(\%)$ | $\sigma_{\rm syst}(\%)$ | $\Sigma(\sigma)$ | $\mathcal{B}_R^{\rm prod}$ |
|---|---|---|---|---|---|---|
| $X(3872) \to \pi^+\pi^- J/\psi$ | $4.8 \pm 15.4$ | 31.4 | 3.26 | 18.7 | 0.3 | $< 9.5 \times 10^{-6}$ |
| $Y(4260) \to \pi^+\pi^- J/\psi$ | $-31.1 \pm 88.9$ | 134.6 | 3.50 | 35.6 | – | $< 3.8 \times 10^{-5}$ |
| $Y(4260) \to \pi^+\pi^-\psi(2S)$ | $6.7 \pm 29.4$ | 56.9 | 0.71 | 35.0 | 0.2 | $< 7.9 \times 10^{-5}$ |
| $Y(4360) \to \pi^+\pi^-\psi(2S)$ | $-25.4 \pm 30.1$ | 45.6 | 0.86 | 50.0 | – | $< 5.2 \times 10^{-5}$ |
| $Y(4660) \to \pi^+\pi^-\psi(2S)$ | $-55.0 \pm 26.2$ | 23.1 | 1.06 | 40.7 | – | $< 2.2 \times 10^{-5}$ |
| $Y(4260) \to K^+K^- J/\psi$ | $-13.7 \pm 10.9$ | 14.5 | 1.91 | 45.8 | – | $< 7.5 \times 10^{-6}$ |
| $Y(4140) \to \phi J/\psi$ | $-0.1 \pm 1.2$ | 3.6 | 0.69 | 11.0 | – | $< 5.2 \times 10^{-6}$ |
| $X(4350) \to \phi J/\psi$ | $2.3 \pm 2.5$ | 7.6 | 0.92 | 10.4 | 1.2 | $< 8.1 \times 10^{-6}$ |
| $Z_c(3900)^\pm \to \pi^\pm J/\psi$ | $-26.5 \pm 39.1$ | 57.5 | 4.39 | 47.3 | – | $< 1.3 \times 10^{-5}$ |
| $Z_c(4200)^\pm \to \pi^\pm J/\psi$ | $-238.6 \pm 154.2$ | 235.1 | 3.87 | 48.4 | – | $< 6.0 \times 10^{-5}$ |
| $Z_c(4430)^\pm \to \pi^\pm J/\psi$ | $94.2 \pm 71.4$ | 195.8 | 3.97 | 34.4 | 1.2 | $< 4.9 \times 10^{-5}$ |
| $Z_c(4050)^\pm \to \pi^\pm\psi(2S)$ | $37.0 \pm 47.7$ | 112.7 | 1.27 | 46.2 | 0.4 | $< 8.8 \times 10^{-5}$ |
| $Z_c(4430)^\pm \to \pi^\pm\psi(2S)$ | $23.2 \pm 42.4$ | 92.0 | 1.35 | 47.1 | 0.1 | $< 6.7 \times 10^{-5}$ |
| $Z_{cs}^\pm \to K^\pm J/\psi$ | $-22.2 \pm 17.4$ | 22.4 | 3.88 | 48.7 | – | $< 5.7 \times 10^{-6}$ |

fraction ($\mathcal{B}$) for each state are listed in Table III, together with the reconstruction efficiencies ($\varepsilon$), the systematic uncertainties ($\sigma_{\rm syst}$), and the signal significances ($\Sigma$); the latter are calculated using $\sqrt{-2\ln(\mathcal{L}_0/\mathcal{L}_{\rm max})}$, where $\mathcal{L}_0$ and $\mathcal{L}_{\rm max}$ are the likelihoods of the fits without and with a signal component, respectively.

Several sources of systematic errors are taken into account in the branching fraction measurements. Tracking efficiency uncertainty is estimated to be 0.35% per track with high momentum and is additive. Based on the measurements of the identification efficiencies of lepton pairs from $\gamma\gamma \to \ell^+\ell^-$ events and pions from a low-background sample of $D^*$ events, MC simulation yields uncertainties of 1.6% for each lepton, 1.4% for each pion, and 1.3% for each kaon. The trigger efficiency evaluated from simulation is greater than 99.9% with an uncertainty that is negligibly small. The difference in the signal yields when the mass and width of each $XYZ$ state are varied by $1\sigma$ is used as an estimate of the systematic error associated with mass and width uncertainties [28]. In the simulation of generic $J/\psi(\psi(2S))$ decays, the unknown decay channels are produced by the Lund fragmentation model in PYTHIA [29]. By generating different sets of MC samples with different relative probabilities to produce the various possible $q\bar{q}$ ($q = u, d, s$) pairs in the $J/\psi(\psi(2S))$ decays, the largest difference in the efficiencies is found to be less than 0.1% and is neglected. The errors on the branching fractions of the intermediate states are taken from the Particle Data Group tables [28]; these are 1.1%, 6.3%, 1.2%, and 1.0% for $J/\psi \to \ell^+\ell^-$, $\psi(2S) \to \ell^+\ell^-$, $\psi(2S) \to \pi^+\pi^- J/\psi$, and $\phi \to K^+K^-$, respectively; the weighted average for the two $\psi(2S)$ decay modes is 3.5%. By varying the background shapes, the order of the Chebyshev polynomial and the fitting range, the deviations of the fitted signal yields for $J/\psi(\psi(2S))$ productions are estimated for each $x$ bin. The upper limits on the signal yields vary by less than 49.4%, depending on the decay mode. The MC statistical errors are estimated using the reconstruction efficiencies and the number of generated events; these are 1.0% or less. The error on the total number of $\Upsilon(1S)$ events is 2.0%. Assuming that all sources are independent, their uncertainties are summed in quadrature. The total systematic errors ($\sigma_{\rm syst}$) for each channel are listed in Table III.

In summary, using the $102 \times 10^6$ $\Upsilon(1S)$ events collected with the Belle detector, distinct $J/\psi$ and $\psi(2S)$ signals are observed in the $\Upsilon(1S)$ inclusive decays. The corresponding branching fractions are measured to be $\mathcal{B}(\Upsilon(1S) \to J/\psi + \text{anything}) = (5.25 \pm 0.13(\text{stat}) \pm 0.25(\text{syst})) \times 10^{-4}$ and $\mathcal{B}(\Upsilon(1S) \to \psi(2S) + \text{anything}) = (1.23 \pm 0.17(\text{stat}) \pm 0.11(\text{syst})) \times 10^{-4}$ with substantially improved precision compared to previous results of $(6.5 \pm 0.7) \times 10^{-4}$ [7,8] and $(2.7 \pm 0.9) \times 10^{-4}$ [7] for $J/\psi$ and $\psi(2S)$, respectively. Several theoretical papers have suggested the study of $J/\psi$ production in $\Upsilon(1S)$ decays as an example of charmonium production mechanisms in gluon-rich environments. Some color-octet [38] and color-singlet [39] models predict $\mathcal{B}(\Upsilon(1S) \to J/\psi + \text{anything})$ of $6.2 \times 10^{-4}$ and $5.9 \times 10^{-4}$, respectively. Our measured value is of the same order as the theoretical estimations. We also search for a variety of $XYZ$ states in $\Upsilon(1S)$ inclusive decays for the first time, where the $XYZ$ candidates of interest are reconstructed from their final states that contain a $J/\psi(\psi(2S))$ and up to two charged light hadrons ($K^\pm/\pi^\pm$). No evident signal is found for any of them and 90% C.L. upper limits are set on the product branching fractions and listed in Table III. There is no striking evidence for previously unseen structures in $K^+K^-\psi(2S)$ and $K^\pm\psi(2S)$ invariant mass distributions.

We thank the KEKB group for the excellent operation of the accelerator; the KEK cryogenics group for the efficient operation of the solenoid; and the KEK computer group, the National Institute of Informatics, and the PNNL/EMSL computing group for valuable computing and SINET4 network support. We acknowledge support from the Ministry of Education, Culture, Sports, Science, and Technology (MEXT) of Japan, the Japan Society for the Promotion of Science (JSPS), and the Tau-Lepton Physics Research Center of Nagoya University; the Australian Research Council; Austrian Science Fund under Grants No. P 22742-N16 and No. P 26794-N20; the National Natural Science Foundation of China under Contracts No. 10575109, No. 10775142, No. 10875115, No. 11175187, No. 11475187 and No. 11575017; the Chinese Academy of Science Center for Excellence in Particle Physics; the Ministry of Education, Youth and Sports of the Czech Republic under Contract No. LG14034; the Carl Zeiss Foundation, the Deutsche Forschungsgemeinschaft, the Excellence Cluster Universe, and the VolkswagenStiftung; the Department of Science and Technology of India; the Istituto Nazionale di Fisica Nucleare of Italy; the WCU program of the Ministry of Education, National Research Foundation (NRF) of Korea Grants No. 2011-0029457, No. 2012-0008143, No. 2012R1A1A2008330, No. 2013R1A1A3007772, No. 2014R1A2A2A01005286, No. 2014R1A2A2A0100 2734, No. 2015R1A2A2A01003280, No. 2015H1 A2A1033649; the Basic Research Lab program under NRF Grant No. KRF-2011-0020333, Center for Korean J-PARC Users, No. NRF-2013K1A3A7A06056592; the Brain Korea 21-Plus program and Radiation Science Research Institute; the Polish Ministry of Science and Higher Education and the National Science Center; the Ministry of Education and Science of the Russian Federation and the Russian Foundation for Basic Research; the Slovenian Research Agency; Ikerbasque, Basque Foundation for Science and the Euskal Herriko Unibertsitatea (UPV/EHU) under program UFI 11/55 (Spain); the Swiss National Science Foundation; the Ministry of Education and the Ministry of Science and Technology of Taiwan; and the U.S. Department of Energy and the National Science Foundation. This work is supported by a Grant-in-Aid from MEXT for Science Research in a Priority Area ("New Development of Flavor Physics") and from JSPS for Creative Scientific Research ("Evolution of Tau-lepton Physics").

[1] N. Brambilla *et al.*, Eur. Phys. J. C **71**, 1534 (2011).
[2] S. Godfrey and S. L. Olsen, Annu. Rev. Nucl. Part. Sci. **58**, 51 (2008).
[3] N. Brambilla *et al.*, Eur. Phys. J. C **74**, 2981 (2014).
[4] C. Z. Yuan, Int. J. Mod. Phys. A **29**, 1430046 (2014).
[5] C. P. Shen *et al.* (Belle Collaboration), Phys. Rev. D **82**, 051504(R) (2010).
[6] X. L. Wang *et al.* (Belle Collaboration), Phys. Rev. D **84**, 071107(R) (2011).
[7] R. A. Briere *et al.* (CLEO Collaboration), Phys. Rev. D **70**, 072001 (2004).
[8] R. Fulton *et al.* (CLEO Collaboration), Phys. Lett. B **224**, 445 (1989).
[9] S. K. Choi *et al.* (Belle Collaboration), Phys. Rev. Lett. **91**, 262001 (2003).
[10] B. Aubert *et al.* (*BABAR* Collaboration), Phys. Rev. Lett. **95**, 142001 (2005).
[11] X. L. Wang *et al.* (Belle Collaboration), Phys. Rev. D **91**, 112007 (2015).
[12] B. Aubert *et al.* (*BABAR* Collaboration), Phys. Rev. Lett. **98**, 212001 (2007).
[13] X. L. Wang *et al.* (Belle Collaboration), Phys. Rev. Lett. **99**, 142002 (2007).
[14] T. E. Coan *et al.* (CLEO Collaboration), Phys. Rev. Lett. **96**, 162003 (2006).
[15] T. Aaltonen *et al.* (CDF Collaboration), Phys. Rev. Lett. **102**, 242002 (2009).
[16] C. P. Shen *et al.* (Belle Collaboration), Phys. Rev. Lett. **104**, 112004 (2010).
[17] M. Ablikim *et al.* (BESIII Collaboration), Phys. Rev. Lett. **110**, 252001 (2013).
[18] Z. Q. Liu *et al.* (Belle Collaboration), Phys. Rev. Lett. **110**, 252002 (2013).
[19] K. Chilikin *et al.* (Belle Collaboration), Phys. Rev. D **90**, 112009 (2014).
[20] S. K. Choi *et al.* (Belle Collaboration), Phys. Rev. Lett. **100**, 142001 (2008).
[21] S. H. Lee, M. Nielsen, and U. Wiedner, J. Korean Phys. Soc. **55**, 424 (2009).
[22] J. M. Dias, X. Liu, and M. Nielsen, Phys. Rev. D **88**, 096014 (2013).
[23] A. Abashian *et al.* (Belle Collaboration), Nucl. Instrum. Methods Phys. Res., Sect. A **479**, 117 (2002).
[24] J. Brodzicka *et al.*, Prog. Theor. Exp. Phys. (2012) 04D001.
[25] S. Kurokawa and E. Kikutani, Nucl. Instrum. Methods Phys. Res., Sect. A **499**, 1 (2003), and other papers included in this volume.
[26] T. Abe *et al.*, Prog. Theor. Exp. Phys. (2013) 03A001 and following articles up to 03A011.
[27] D. J. Lange, Nucl. Instrum. Methods Phys. Res., Sect. A **462**, 152 (2001).
[28] K. A. Olive *et al.*, Chin. Phys. C **38**, 090001 (2014).
[29] T. Sjostrand, S. Mrenna, and P. Skands, J. High Energy Phys. 05 (2006) 026.
[30] K. Abe *et al.* (Belle Collaboration), Phys. Rev. D **70**, 071102 (2004).
[31] E. Nakano, Nucl. Instrum. Methods Phys. Res., Sect. A **494**, 402 (2002).

[32] A. Abashian *et al.*, Nucl. Instrum. Methods Phys. Res., Sect. A **491**, 69 (2002).
[33] K. Hanagaki, H. Kakuno, H. Ikeda, T. Iijima, and T. Tsukamoto, Nucl. Instrum. Methods Phys. Res., Sect. A **485**, 490 (2002).
[34] K. Y. Liu, Z. G. He, and K. T. Chao, Phys. Rev. D **69**, 094027 (2004).
[35] F. Yuan, C. F. Qiao, and K. T. Chao, Phys. Rev. D **56**, 321 (1997).
[36] K. T. Chao, Z. G. He, D. Li, and C. Meng, arXiv:1310.8597; C. Meng (private communication).
[37] In common high-energy physics usage, this Bayesian interval has been reported as a "confidence interval," which is a frequentist-statistics term.
[38] M. Napsuciale, Phys. Rev. D **57**, 5711 (1998).
[39] S. Y. Li, Q. B. Xie, and Q. Wang, Phys. Lett. B **482**, 65 (2000).